Temperature- and pressure-dependent metallic states in (BEDT-TTF)$_8$[Hg$_4$Br$_{12}$(C$_6$H$_5$Br)$_2$]

Alain Audouard,[1,*] Fabienne Duc,[1] David Vignolles,[1] Rustem B. Lyubovskii,[2] Laure Vendier,[3] Gena V. Shilov,[2] Elena I. Zhilyaeva,[2] Rimma N. Lyubovskaya,[2] and Enric Canadell[4]

[1]*Laboratoire National des Champs Magnétiques Intenses (UPR 3228 CNRS, INSA, UJF, UPS) 143 avenue de Rangueil, F-31400 Toulouse, France*

[2]*Institute of Problems of Chemical Physics, RAS, RU-142432 Chernogolovka, MD, Russia*

[3]*CNRS, LCC (Laboratoire de Chimie de Coordination), 205 route de Narbonne, F-31077 Toulouse, France*

[4]*Institut de Ciència de Materials de Barcelona, CSIC, Campus de la UAB, E-08193, Bellaterra, Spain*

(Received 21 March 2011; revised manuscript received 17 May 2011; published 5 July 2011)

Temperature-driven metal-insulator and pressure-driven insulator-metal transitions observed in (BEDT-TTF)$_8$[Hg$_4X_{12}$(C$_6$H$_5Y$)$_2$] with $X = Y =$ Br are studied through band-structure calculations based on x-ray crystal-structure determination and Shubnikov–de Haas (SdH) oscillation spectra, respectively. In connection with the chemical pressure effect, the transition, which is not observed for $X =$ Cl, is due to a gap opening linked to structural changes as the temperature decreases. Even though many-body interactions can be inferred from the pressure dependence of the SdH oscillation spectra, all the data can be described within a Fermi-liquid picture.

DOI: 10.1103/PhysRevB.84.045101 PACS number(s): 71.20.Rv, 61.50.Ks, 71.18.+y, 71.30.+h

I. INTRODUCTION

According to room-temperature x-ray diffraction data,[1–3] the four charge-transfer salts (BEDT-TTF)$_8$[Hg$_4$X$_{12}$(C$_6$H$_5$Y)$_2$] (where $X,Y =$ Cl,Br and BEDT-TTF stands for bisethylenedithiotetrathiafulvalene) are isostructural compounds. In the following, they are referred to as (X,Y). Even though a metallic ground state is observed for both (Cl, Cl) and (Cl, Br), i.e., $X =$ Cl, a metal-insulator transition is reported as the temperature is lowered for $X =$ Br.[4] Band-structure calculations yield a Fermi surface (FS) composed of one electron and one hole compensated quasi-two-dimensional orbits for both (Cl, Cl) (Ref. 5) and (Cl, Br) (Ref. 6), referred to as the α orbits (see Fig. 1). Quantum oscillation spectra of these compounds yield frequencies $F_\alpha = 241.5 \pm 2.0$ T for (Cl, Cl) (Ref. 7) and 235.5 ± 1.0 T for (Cl, Br) (Refs. 6,8, and 9), which correspond to orbit areas of 11% and 16% of the first Brillouin zone (FBZ) area, respectively, in satisfactory agreement with band-structure calculations. In a large enough magnetic field, the orbits are connected by MB junctions. As a result, these FSs can be regarded as textbook cases for the study of quantum oscillations in networks of compensated orbits.[10] In line with this statement, numerous Fourier components that are linear combinations of F_α and of the frequencies linked to the δ and Δ pieces (see Fig. 1) are observed in the quantum oscillation spectra of these two compounds.

Oppositely, both (Br, Cl) and (Br, Br) have an insulating ground state.[4] Nevertheless, a metallic ground state is recovered for (Br, Br) under an applied pressure of 0.4 GPa, and Shubnikov–de Haas (SdH) oscillations have been observed at 0.8 GPa in fields below 15 T.[11] Their frequency ($F = 215$ T) is close to that linked to the closed orbits α of the compounds with $X =$ Cl, i.e., with a metallic ground state at ambient pressure. This could suggest that the pressure-induced metallic state in (Br, Br) is similar to the ambient pressure ground state of (Cl, Cl) and (Cl, Br) and offers the possibility to study the applied pressure-induced evolution of the ground state. In that respect, metal-insulator transitions in strongly correlated fermion systems have received much attention. As an external parameter, such as doping or applied pressure, is varied, numerous phases, such as the Mott insulator, superconducting and density wave states, eventually including quantum critical points, are observed. As examples, quantum critical points have been inferred from the doping dependence of the effective mass in both superconducting cuprates[12] and iron pnictides.[13]

In this paper, we focus first on the temperature dependence of atomic and electronic structures of (Br, Br) in order to get information about the metal-insulator transition. It is concluded that the insulating state at ambient pressure is related to progressive band separation linked to chemical pressure as the temperature decreases, followed by a subtle conformational change in two of the donors in the vicinity of the transition, leading to gap opening. In the second step, the pressure-induced metallic state is considered. The FS topology deduced from SdH oscillation spectra is different from the FS in the metallic state at room temperature but is similar to that of the compounds with $X =$ Cl, indicating that applied pressure and temperature increase have different effects. Finally, even though an increase in many-body effects is observed as approaching the insulating state as the applied pressure decreases, the data are in line with a Fermi-liquid picture throughout the pressure range explored.

II. EXPERIMENTAL

The crystals studied were synthesized by the electrocrystallization technique reported in Ref. 4. Their mean dimensions were $0.1 \times 0.1 \times 0.02$ mm^3 for x-ray diffraction experiments and $0.5 \times 0.5 \times 0.02$ mm^3 for magnetoresistance measurements.

Single-crystal x-ray diffraction data were collected at selected temperatures (100, 120, 150, 200, and 293 K) with an Oxford diffraction Xcalibur charge-coupled device diffractometer equipped with a cryojet cooler device from Oxford Instruments and using a graphite-monochromated Mo-Kα radiation source ($\lambda = 0.71073$ Å). The unit-cell determination

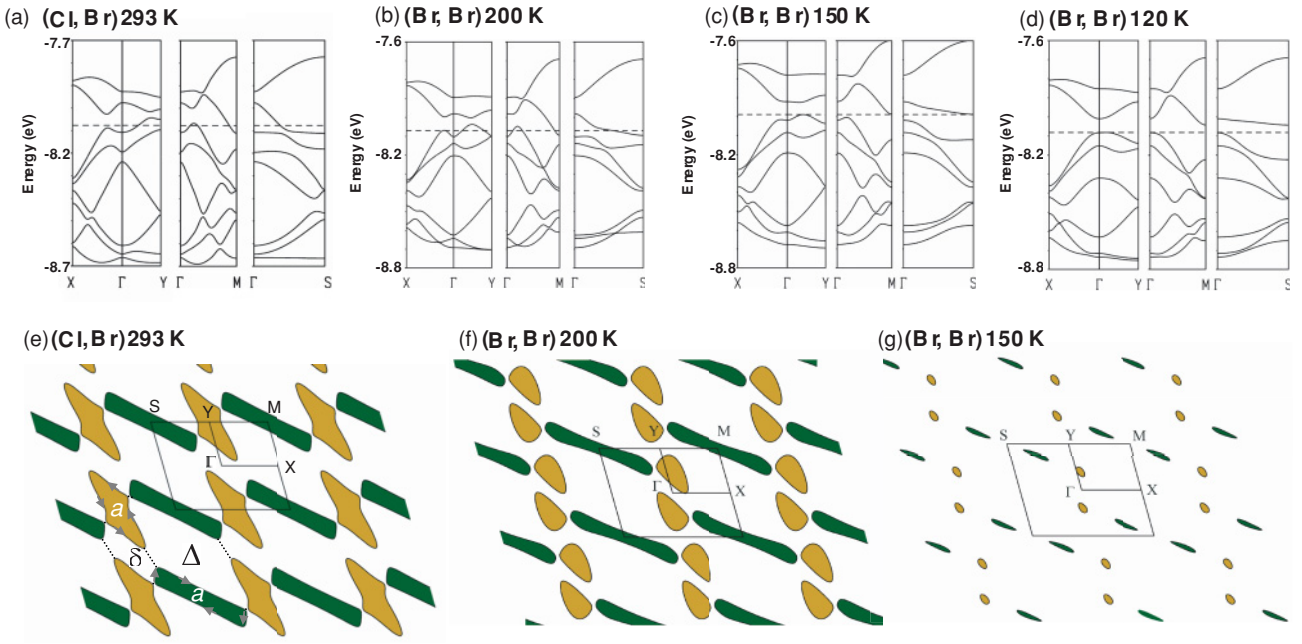

FIG. 1. (Color online) Band structure of (a) (Cl, Br) at 293 K, (b)–(d) (Br, Br) at 200, 150, and 120 K, respectively. Dashed lines mark the Fermi level in (a)–(c) and the top of the highest occupied molecular orbital (HOMO) band in (d). Corresponding FSs of (e) (Cl, Br) at 293 K and (f) and (g) (Br, Br) at 200 and 150 K, respectively. Dark green (dark gray) and tan (light gray) areas stand for electron and hole orbits, respectively. Dashed lines in (e) mark the magnetic breakdown (MB) gaps; labels a depict the closed electron and hole orbits (arrows indicate the quasiparticle path), which have the same area; δ and Δ are forbidden orbits liable to enter MB orbits. Data for (Cl, Br) are from Ref. 6.

and data reduction were carried out using the CRYSALISPRO package.[14] Absorption correction was performed using the multiscan procedure. All the structures were solved by direct methods using SIR92 (Ref. 15) and were refined with the JANA2006 program.[16] All atoms except carbon were refined anisotropically. The hydrogen atoms were not placed in either structure. Experimental details on the crystallographic data and structure refinements are given in Table I. Besides the complete data collections described above, the temperature dependence of cell parameters was obtained by refining the position of 250–400 reflections between 100 and 300 K with temperature steps in the range of 10–25 K.

Tight-binding band-structure calculations were based upon the effective one-electron Hamiltonian of the extended Hückel method.[17] A modified Wolfsberg-Helmholtz formula was used to calculate the nondiagonal H_{ij} values.[18] All valence electrons were taken into account in the calculations, and the basis set consisted of Slater-type orbitals of double-ζ quality for C $2s$ and $2p$, S $3s$ and $3p$, and of single-ζ quality for H. The ionization potentials, contraction coefficients and exponents were taken from previous works.[5,19]

Alternating current (1 μA, 77 Hz) and (5–10 μA, 20 kHz) was injected parallel to the normal to the conducting plane for measurements of the interlayer zero-field resistance and magnetoresistance, respectively. Electrical contacts to the crystal were made using annealed platinum wires of 20 μm in diameter glued with graphite paste. Hydrostatic pressure was applied up to 1.0 GPa in an anvil cell designed for isothermal measurements in pulsed magnetic fields.[20] In the following, the pressure applied at room temperature is considered.

TABLE I. Experimental data and agreement factors for the structure refinements of $(BEDT\text{-}TTF)_8[Hg_4Br_{12}(C_6H_5Br)_2]$ at 100, 120, 150, 200 and 293 K. Reflections with $I > 3\sigma(I)$ were considered as observed [$\sigma(I)$ corresponds to the estimated standard deviations of measured individual intensities I].

Temperature (K)	100	120	150	200	293
Maximum θ (deg)	32	29	32	29	32
Redundancy	1.65	2.81	1.67	2.83	1.70
Number of measured reflections (observed/all)	18 078/37 105	24 105/48 089	18 582/38 435	19 996/48 673	13 408/40 197
Unique reflections (observed/all)	10 560/22 447	9025/17 107	10 796/22 940	7345/17 186	7151/23 540
R_{int} (observed/all)	6.82/8.79	3.98/4.89	3.96/4.97	4.15/5.70	6.09/9.00
Rw_{obs}/Rw_{all}	8.75/9.14	2.93/3.10	5.91/6.13	3.76/4.02	8.81/8.89
goodness of fit (obs)/goodness of fit (all)	3.57/2.53	1.16/0.88	2.40/1.69	1.47/1.01	3.71/2.11
Number of refined parameters	554	554	554	554	554

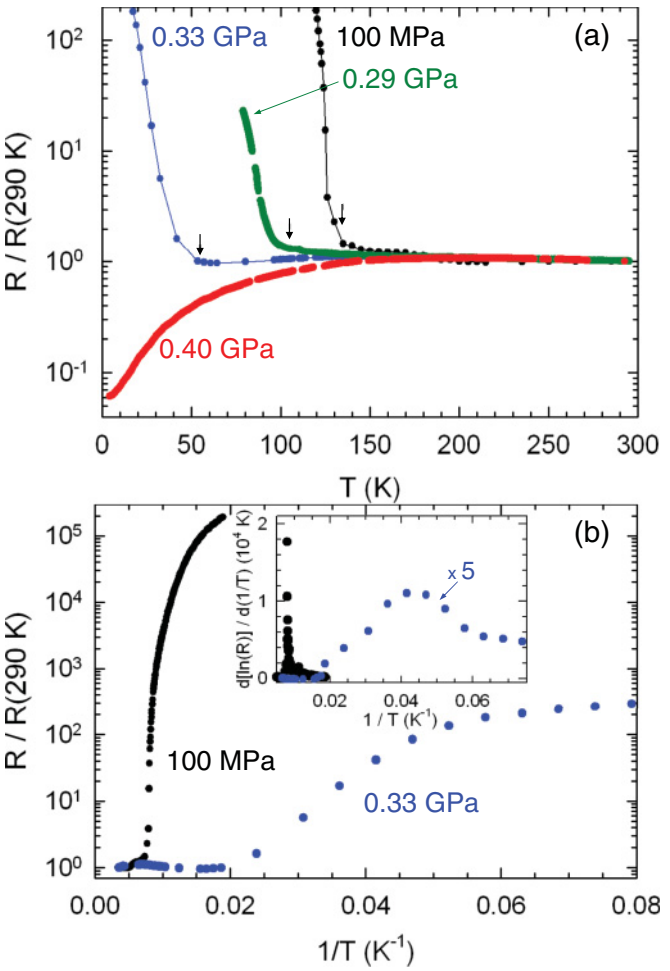

FIG. 2. (Color online) (a) Temperature dependence of the zero-field resistance at a few applied pressures. Arrows indicate the onset of the resistance rise on cooling (T_{onset}). (b) Arrhenius plot of the resistance at ambient pressure and 0.33 GPa. The maximum of the logarithmic derivative displayed in the inset yields the temperature T_c.

Magnetoresistance experiments were performed up to 55 T in pulsed magnetic fields with a pulse decay duration of 0.36 s in the temperature range from 1.5 to 4.2 K. Magnetic fields were applied normal to the conducting plane. A lock-in amplifier with a time constant of 30 μs was used to detect the signal across the potential contacts. Analysis of the oscillatory magnetoresistance is based on discrete Fourier transforms of the data, calculated with a Blackman window.

III. ZERO-FIELD PROPERTIES

At ambient pressure, a strong increase in the zero-field resistance is observed in Fig. 2(a) as the temperature is lowered. No hysteresis is detected upon heating. The Arrhenius plot of these data exhibits a clear inflection point as reported in Fig. 2(b). Therefore, the metal-insulator transition temperature ($T_c = 122 \pm 5$ K) can be obtained through the sharp maximum of the parameter $d[\ln(R)]/d(1/T)$. More insight into this behavior can be obtained through x-ray diffraction data. $(BEDT\text{-}TTF)_8[Hg_4Br_{12}(C_6H_5Br)_2]$ crystallizes in the triclinic crystal system, space group $P\bar{1}$. Upon lowering the temperature

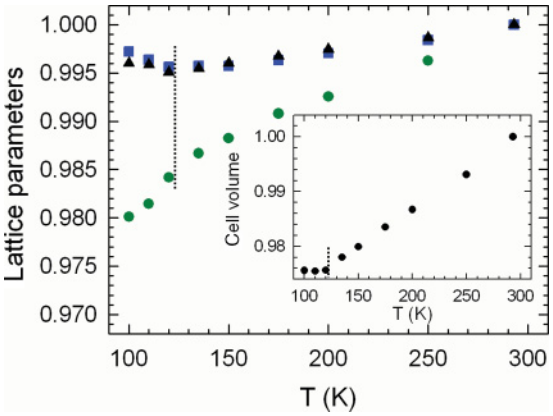

FIG. 3. (Color online) Temperature dependence of lattice parameters a (circles), b (squares), and c (triangles). Data are normalized to their values at 293 K. Corresponding data for the unit-cell volume is displayed in the inset. Vertical lines mark $T_c = 122$ K deduced from zero-field resistance measurements at the ambient pressure of Fig. 2.

to 100 K, no symmetry change is observed. However, the temperature dependence of the cell parameters and volume reported in Fig. 3 exhibit a kink at T_c, which indicates that the transition is linked to a structural change.

To gain some insight into the origin of this change, the evolution of the crystal structure can be considered as the temperature is lowered from room temperature. However, in view of the large number of structural parameters associated with the big unit cell ($V_{cell} = 3720$ A^3 at room temperature) that should account for the relatively small change evidenced in the data of Fig. 3, it seems difficult to extract information from a structural study alone. Under such circumstances, it is usually more informative to consider the electronic structure first. Because of the directionality of the S and C p orbitals leading to the HOMO of BEDT-TTF, the HOMO-HOMO intermolecular interactions are quite sensitive to small structural variations, and their analysis is extremely useful for understanding the relationship between features of the crystal and the electronic structures (see, e.g., Refs. 21 and 22). The so-called $\beta_{HOMO\text{-}HOMO}$ intermolecular interaction energies[23] for the different donor-donor interactions, as well as the HOMO energies of the different BEDT-TTF donors as a function of temperature, are considered in the following. As shown in Fig. 4, the donor lattice of the present salt contains 4 different BEDT-TTF molecules and 14 different intermolecular interactions. Five of the interactions (I–V) are lateral π-π interactions, four (VI–IX) are interactions within the stacks running along the (a-b) direction, and five (X–XIV) are interactions along the step chains, which are usually the strongest for this type of lattice. The different $|\beta_{HOMO\text{-}HOMO}|$ values and HOMO energies calculated at 200, 150, and 120 K are reported in Table II. Let us note that the three crystal structures on which these calculations are based on were determined for the same crystal.

Regarding $|\beta_{HOMO\text{-}HOMO}|$ interactions, three different types of behavior can be distinguished in Table II: (i) interactions, such as IX, which exhibit a monotonous gradual change, (ii) interactions, such as I, III, IV, etc., which gradually change to reach a saturation around 150 K, and (iii) interactions, such as II, VII, and X (and, to a lesser extent, XIII)

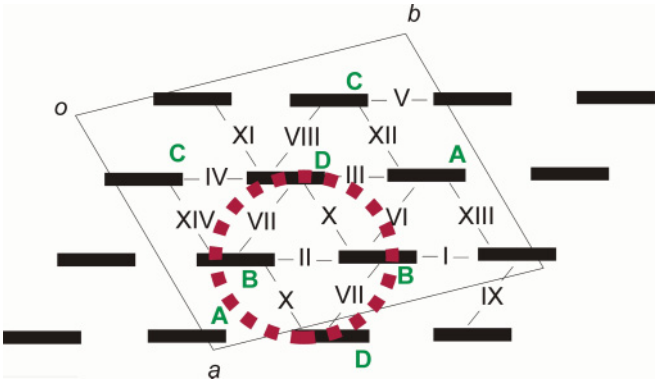

FIG. 4. (Color online) Donor lattice of (BEDT-TTF)$_8$[$Hg_4Br_{12}(C_6H_5Br)_2$] where capital letters and roman numerals label the different types of donors and intermolecular interactions, respectively. The ellipse in the dotted line highlights the part of the lattice where main structural changes should occur according to the electronic structure data.

exhibiting a large nonmonotonic change, in particular, at low temperatures. Whereas, behaviors (i) and (ii) are observed in most organic conductors under thermal contraction, behavior (iii) is *atypical* and certainly points to some abrupt change at low temperatures. According to Fig. 4, the three interactions II, VII, and X, which clearly exhibit this atypical change are all clustered in the region of interaction between donors B and D. Besides, contrary to donors A and C, the temperature dependence of the HOMO energy of B and D is strongly nonmonotonic as well. Therefore, it is clear that some abrupt change affecting the electronic parameters occurs in the region highlighted in Fig. 4 around the four donors of types B and D.

TABLE II. Calculated values of $|\beta_{\text{HOMO-HOMO}}|$ for the 14 different donor-donor interactions and HOMO energies (eV) of the 4 different donors of (BEDT-TTF)$_8$[$Hg_4Br_{12}(C_6H_5Br)_2$]. Labels are the same as in Fig. 4.

	$\lvert\beta_{\text{HOMO-HOMO}}\rvert$ (eV)		
Interaction	200 K	150 K	120 K
I	0.1312	0.1385	0.1383
II	0.1093	0.1113	0.1000
III	0.1434	0.1560	0.1525
IV	0.1328	0.1416	0.1418
V	0.1197	0.1290	0.1222
VI	0.1132	0.1319	0.1345
VII	0.1299	0.1061	0.1284
VIII	0.0719	0.0863	0.0847
IX	0.1135	0.1158	0.1193
X	0.2915	0.2938	0.2861
XI	0.1649	0.1565	0.1312
XII	0.2257	0.2385	0.2364
XIII	0.2897	0.2928	0.2820
XIV	0.3066	0.3273	0.3242
	HOMO energy (eV)		
Donor	200 K	150 K	120 K
A	−8.4917	−8.5048	−8.5767
B	−8.4808	−8.3775	−8.4266
C	−8.4687	−8.4443	−8.4492
D	−8.4738	−8.4561	−8.6004

Taking advantage of these results, we can examine the evolution of the crystal structure as the temperature is varied. At variance with the other structural parameters, the temperature dependence of the outer C-C single-bond length of the outer six-membered rings of donors B and D is large and nonmonotonic. Most interestingly, these features are related with a conformational change affecting these six-membered rings, which change as displayed in Fig. 5. The same change was also observed in another set of structural refinements for a different crystal. Consequently, with both the crystallographic and the electronic structure results in mind, we can quite firmly conclude that the structural change occurring around 122 K is related to a conformational change in two of the BEDT-TTF donors and leads to the kink in Fig. 3.

According to the band-structure calculations reported in Fig. 1, a metallic state is obtained in the high-temperature range. At room temperature and 200 K, the FS is composed of one elongated electron orbit with an area $A_e = 13\%$ of the FBZ area and two hole orbits with area $A_h = A_e/2$. Although this topology is different from that of (Cl, Br) displayed in Fig. 1(e), it can be regarded as closely related, the only qualitative difference being a splitting of the hole orbit. In particular, we are still dealing with a compensated metal. As the temperature is lowered, a sizable shrinkage of the orbit area is observed since, at 150 K, the electron orbits are also split in two parts with an area that reduces to only 1% of the FBZ area each. Further temperature lowering finally leads to gap opening [$E_g = 38$ meV at 120 K, see Fig. 1(d)] and to the orbits' suppression, accounting for the metal-insulator transition observed in the ambient pressure data of Fig. 2. The difference between the behavior of (Cl, Br) and (Br, Br) can be accounted for by chemical pressure. Indeed, since Br atoms entering the HgX_3 anions are larger than Cl atoms, the distance between BEDT-TTF molecules is larger for $X = \text{Br}$ than for $X = \text{Cl}$. As a result, band overlapping is less pronounced in (Br, Br), leading to a less conducting compound and leaving enough room for molecular changes or sliding as the temperature decreases. Coming back to the origin of the metal-to-insulator transition, we conclude that thermal contraction prepares the system by considerably reducing the band overlap. At T_c, this overlap is already quite small, and a sudden conformational change in half the donor molecules leads to the band-gap opening, hence, to the abrupt change in the conductivity regime reported in Fig. 2.

As the applied pressure increases, T_c decreases, the transition broadens, and the ground state becomes clearly not insulating at pressures of a few tenths of a GPa, as displayed in Fig. 2(b). As a result, the temperature at which the resistance starts to increase on cooling (T_{onset}) is significantly higher than T_c in this pressure range. Nevertheless, both T_c and T_{onset} go to zero at $P_c = 0.34 \pm 0.02$ GPa as observed in Fig. 6.

The temperature dependence of the resistivity in the pressure-induced metallic state is very similar to the data obtained for (Cl, Br).[6] More precisely, a bump is observed followed by a metallic behavior [see Fig. 7(a)]. This behavior, observed in many correlated organic conductors, is attributed to a combined influence of disorder and electron

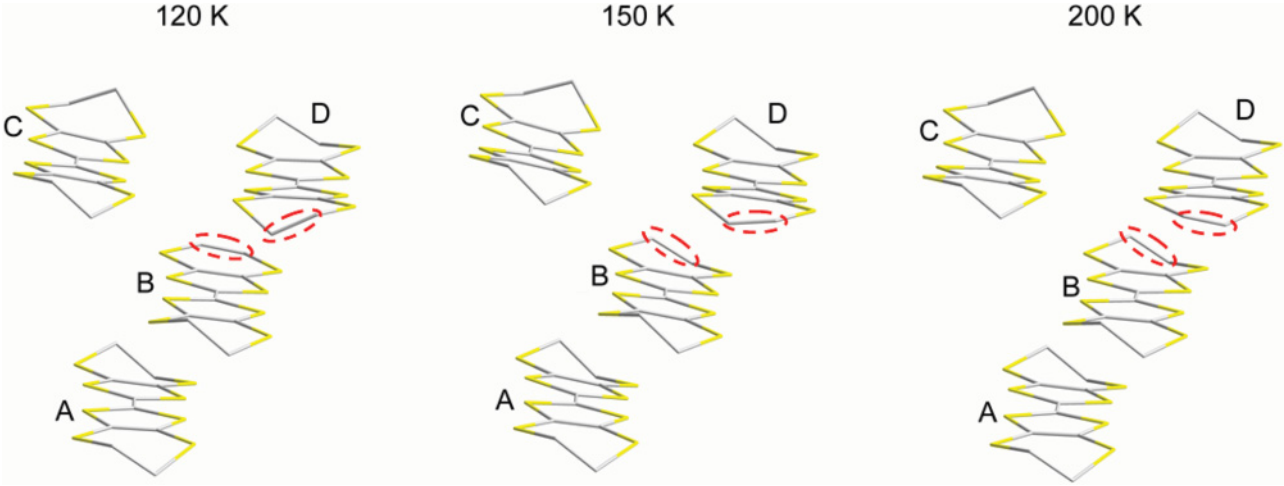

FIG. 5. (Color online) Evolution of the BEDT-TTF molecules conformation as a function of temperature. Labels are the same as in Fig. 4. Ellipses in the dotted lines mark the C-C bonds that experience the most significant changes as the temperature varies (see text).

correlations.[6,24–27] Below about 25 K, the resistivity follows a T^2 variation [$\rho = \rho_0 + AT^2$, see Fig. 7(b)], which is generally regarded as a signature of a correlated Fermi liquid. As already observed for the (Cl, Br) compound, the A coefficient strongly decreases as the applied pressure increases, suggesting a reduction of many-body strength under pressure.[6]

IV. FIELD-DEPENDENT PROPERTIES UNDER PRESSURE

As displayed in Fig. 8, SdH oscillations are observed in the pressure-induced metallic state. Fourier analysis reveals a mean peak that ranges from 205 ± 2 T at 0.4 GPa to 225.5 ± 1.0 T at 1.0 GPa (see Fig. 9). These values correspond to 9.5% and 10.5% of the ambient pressure FBZ area at 200 K, respectively, which is close to the a orbit area of (Cl, Cl) and (Cl, Br) and to the ambient pressure electron orbit area of (Br, Br) deduced from band-structure calculations at 200 K. The pressure sensitivity of this frequency is much larger than for (Cl, Br), namely, $d[\ln(F_a)]/dP = 0.20$ GPa^{-1} and 0.04 GPa^{-1} for (Br, Br) and (Cl, Br), respectively. In the case

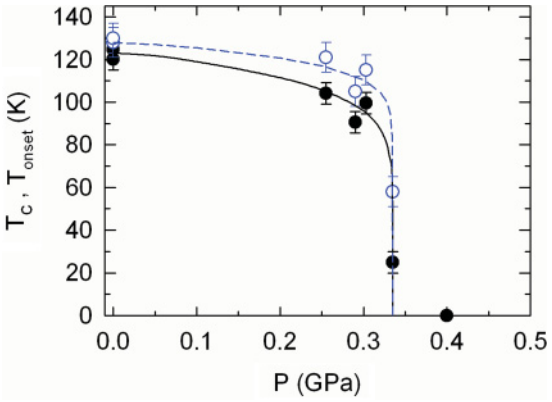

FIG. 6. (Color online) Applied pressure dependence of T_c (solid symbols) and T_{onset} (open symbols) as defined in Fig. 2. Lines are guides to the eye.

of (Cl, Br), the frequency linked to the quantum interferometer b, the area of which is just equal to the FBZ area ($F_b = 2F_a + F_\delta + F_\Delta$), is detected in the spectra. Since the same pressure dependence is observed for F_b and F_a, it can be concluded that the pressure dependence of F_a is the same as that of the FBZ area. In the case where this statement holds for (Br, Br), it indicates that the FBZ area, hence, the unit-cell parameters of (Br, Br), are more strongly pressure sensitive. The effect of chemical pressure can also be invoked to account for this difference in pressure sensitivity.

Two other points must be noticed. First, band-structure calculations relevant to the metallic state at ambient pressure in the temperature range above T_c predict split-hole orbits (see Fig. 1), hence, a frequency $F_a/2$. Second, oscillatory spectra of Fig. 8 contain much less Fourier components than in the case of (Cl, Cl) and (Cl, Br). Indeed, apart from the frequency F_a and its second harmonics, only a frequency at 770 ± 20 T is observed at 1 GPa. Regarding the first point, it can be remarked that, due to the rather small field range in which oscillations are observed, Fourier peaks are rather broad, which makes it necessary to check if they actually correspond to a single frequency (see, e.g., Ref. 28).

More insight into these two points can be obtained through field and temperature dependences of the a oscillation amplitude. In the following, this is considered in the framework of the Lifshitz-Kosevich model, the main ingredients of which are the effective mass (m^*), the Dingle temperature, which is linked to the scattering rate ($T_D = \hbar/2\pi k_B \tau$), and the MB field ($B_0$).

Figure 10 displays oscillatory magnetoresistance data at 0.4 GPa, which is the studied applied pressure closest to P_c, and the best fittings to the data assuming only one Fourier component is involved. Good agreement between fits and experimental data is observed for both the oscillatory magnetoresistance and the corresponding Fourier analysis. This result demonstrates that no Fourier component with frequency $F_a/2$ enters the oscillatory spectrum. Therefore, the data are more in line with a Fermi surface, such as that of (Cl, Cl) and (Cl, Br), i.e., composed of one electron and one hole compensated orbit.

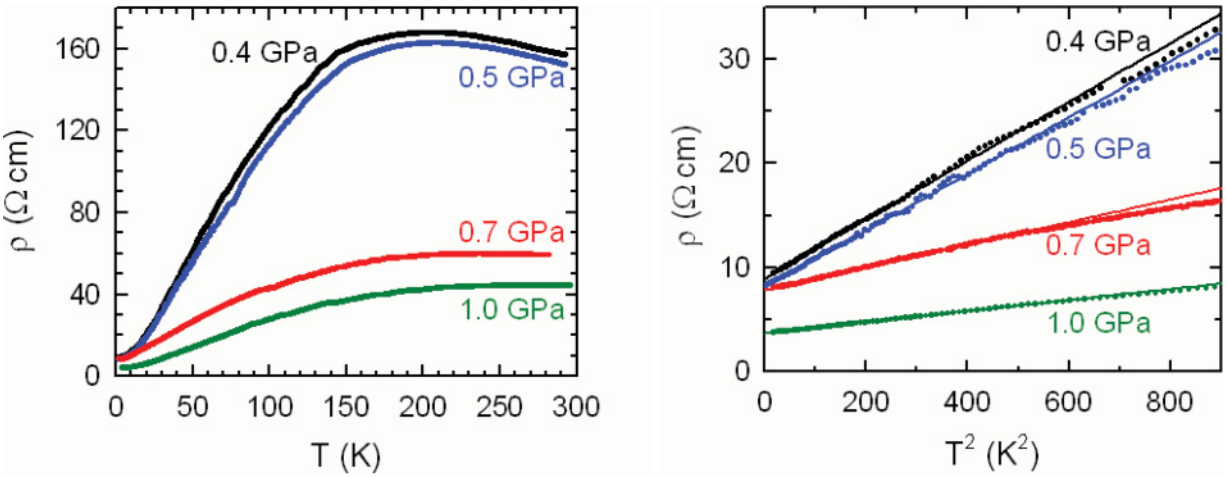

FIG. 7. (Color online) (a) Temperature dependence of the resistivity in the pressure-induced metallic state above P_c and (b) low-temperature part of the data plotted as a function of T^2.

As reported in Fig. 9(b), $m^*(a)$ strongly increases as the applied pressure decreases, as observed for (Cl, Br). In this latter case, the A coefficient of the zero-field resistivity is proportional to $[m^*(a)]^2$, which has been interpreted on the basis of a pressure-induced decrease in electron correlations.[6,25] Although only a very rough agreement with this proportionality is observed for (Br, Br), A strongly decreases as the applied pressure decreases, as observed in Fig. 7(b). This feature suggests that applied pressure induces a decrease in the electron correlations as well.

In the pressure range from 0.4 to 0.7 GPa, the Dingle plots of Fig. 11 exhibit a linear behavior, which allow deducing Dingle temperatures in the range of 6 to 7 K. In contrast, a clear curvature is observed at 1.0 GPa. This curvature, which is concomitant with the appearance of the frequency at 770 ± 20 T in the spectra, can be accounted for by the decrease in the MB field, hence, of the field-dependent MB damping factor, which includes four Bragg reflections for the a oscillations ($R_{MB} = [1 - \exp(-B_0/B)]^2$).[8] Within this assumption, the frequency at 770 T might correspond to the MB orbit $2a + \delta$, in which case, the frequency linked to δ amounts to $F_\delta = 319 \pm 22$ T, which is very large compared to the data of (Cl, Br). Nonetheless, the effective mass linked to this frequency is 1.3 ± 0.2, which is close to $2m^*(a)$, as expected for $m^*(2a + \delta)$.[8] Unfortunately, a reliable value of the MB field cannot be derived from the data due to the large Dingle temperature.[30] Nevertheless, it can be inferred that the MB field decreases as the applied pressure increases, as already observed for (Cl, Br). However, the MB field is much larger in (Br, Br) than in (Cl, Br) at a given applied pressure (see Ref. 6 and open symbols in Fig. 11), which justifies the absence of frequency mixing in (Br, Br).

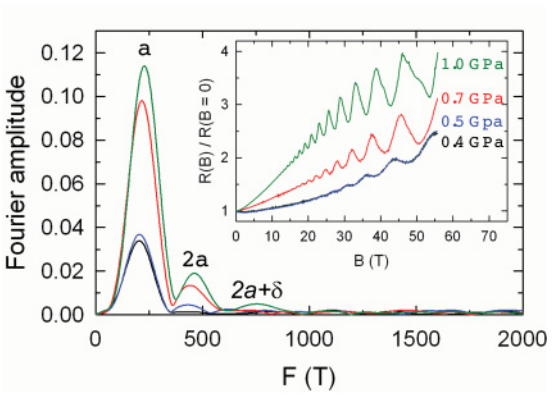

FIG. 8. (Color online) Fourier analysis of the magnetoresistance data at 1.5 K displayed in the inset. Labels refer to the FS displayed in Fig. 1.

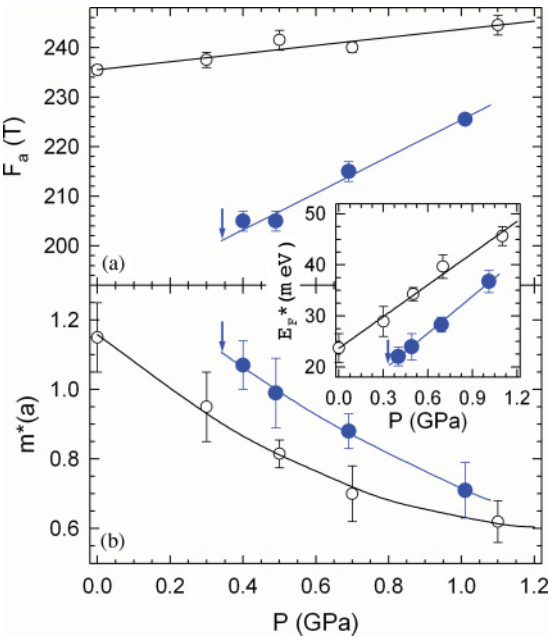

FIG. 9. (Color online) Applied pressure dependence of (a) the oscillation frequency F_a and (b) the effective mass $m^*(a)$. The Fermi energy calculated as $E_F^* = e\hbar F_a/m^*(a)$ is displayed in the inset. Solid and open symbols stand for (Br, Br) and (Cl, Br), respectively. Arrows mark the critical pressure P_c. Data for (Cl, Br) are from Ref. 6.

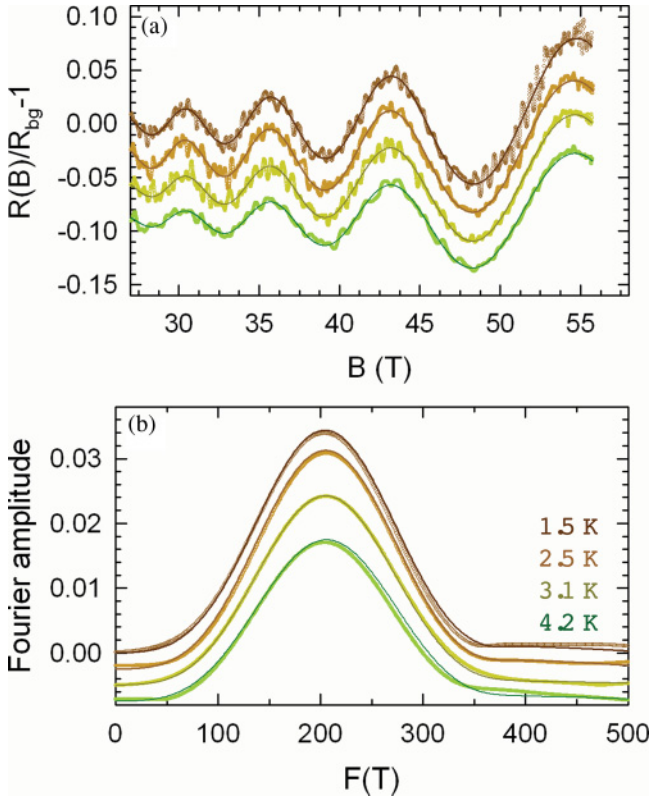

FIG. 10. (Color online) (a) Oscillatory magnetoresistance data at 0.4 GPa and best fits of the Lifshitz-Kosevich formalism obtained with $F_a = 205$ T, $m^*(a) = 1.04$, and $T_D = 7$ K. (b) Corresponding Fourier analysis. Symbols and solid lines stand for experimental data and fits, respectively.

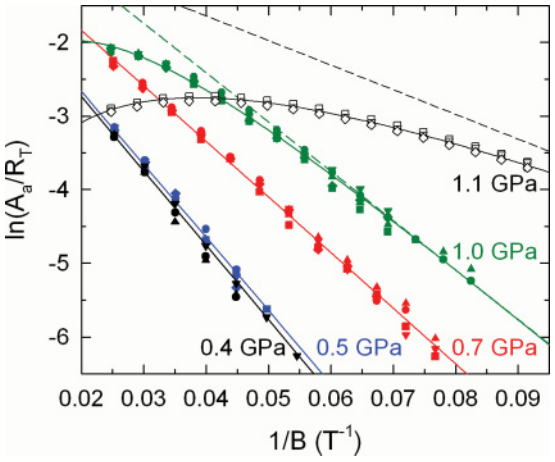

FIG. 11. (Color online) Dingle plots of the a oscillations. Thermal damping factors (R_T) are calculated with the effective masses reported in Fig. 9. Solid and empty symbols are experimental data of (Br, Br) and (Cl, Br), respectively, for various temperatures in the range of 1.5–4.2 K. Solid and dashed lines are best fits of the Lifshitz-Kosevich formalism to the data, including and excluding the contribution of MB, respectively. The MB field (B_0) is infinitely large for (Br, Br) below 1 GPa (i.e., $R_{MB} = 1$), while $B_0 = 50$ and 21 T for (Br, Br) at 1.0 GPa and (Cl, Br) at 1.1 GPa,[6] respectively.

Finally, as is the case for (Cl, Br), the effective mass strongly decreases as the applied pressure increases. Such a variation, which is much too large to be accounted for by any band mass decrease under pressure,[6,25] can be attributed to a pressure-induced decrease in electron correlations since the A coefficient of the T^2 law of the zero-field resistivity also strongly decreases under pressure. Phase diagrams of strongly correlated systems in which insulating, magnetic, superconducting, and non-Fermi liquid states are observed, also exhibit a large overlinear increase or even a divergence of the effective mass as approaching the metal-insulator transition. As pointed out in Ref. 12, this behavior can be more clearly evidenced considering an effective Fermi energy $E_F^* = e\hbar F_a/m^*(a)$, which includes both the effective mass, eventually renormalized by interactions, and the electronic density through the oscillation frequency. As examples, this parameter goes to zero at specific doping values in underdoped superconducting cuprates for which quantum critical points are suggested[12] and at the superconducting-spin-density-wave transition in iron pnictides $BaFe_2(As_{1-x}P_x)_2$.[13] At a variance with the above examples and with numerous strongly correlated fermion systems, the studied compound contains no magnetic atom, and no superconducting ground state is observed in the (temperature-pressure) phase diagram, at least down to 1.5 K. As evidenced in Fig. 9, despite the large pressure sensitivity in the effective mass, E_F^* remains finite at P_c, which is in line with a Fermi-liquid picture.

V. SUMMARY AND CONCLUSION

According to band-structure calculations relevant to the ambient pressure state in the high-temperature range, the FS of (Br, Br) is composed of one electron orbit with area $A_e = 13\%$ of the FBZ area and two hole orbits with area $A_e/2$. This topology is closely related to that of (Cl, Cl) and (Cl, Br), although the hole orbit is not split in the latter cases. As the temperature decreases, the orbits' area strongly decreases leading to a gap opening below $T_c = 122$ K, in line with the temperature dependence of the resistance. This behavior, which is not observed in (Cl, Cl) and (Cl, Br), can be attributed to a chemical pressure effect in which Br atoms of the $[HgBr_3]^-$ anions, larger than Cl atoms, reduce the compression of the donor molecules. As a result, band overlapping is reduced, which accounts for the different FS topologies at room temperature. Besides, as the temperature is lowered, a change in two of the BEDT-TTF molecules conformation and a nonmonotonous temperature dependence of the lattice parameters around T_c are observed.

A pressure-induced metallic ground state is observed above $P_c = 0.34$ GPa. SdH oscillation spectra, observed in the pressure range between 0.4 and 0.7 GPa, exhibit only one Fourier component and its second harmonic. Frequencies are in agreement with both band-structure calculations in the high-temperature range for the electron orbits of (Br, Br) and data for the compensated orbits of (Cl, Cl) and (Cl, Br). No Fourier component with frequency $F_a/2$ is observed, which suggests that the FS under pressure is similar to that of (Cl, Cl) and (Cl, Br). The large pressure sensitivity of F_a, and likely of the FBZ area, can be ascribed to the reduced chemical pressure as well.

Effective mass and coefficient of the T^2 law of the zero-field resistivity strongly decrease as the applied pressure increases. As in the case of (Cl, Br), this can be attributed to a pressure-induced decrease of many-body effects. Nevertheless, at a variance with more strongly correlated systems for which a superconducting state is generally observed in the vicinity of the insulating state in the phase diagram, the effective Fermi energy remains finite at P_c, which is in line with a Fermi-liquid picture throughout the phase diagram of the studied charge-transfer salt family.

ACKNOWLEDGMENTS

This work has been supported by FP7 I3 EuroMagNET II, DGI-Spain (Grants No. FIS2009-12721-C04-03 and No. CSD2007-00041) and RFBR Grant No. 11-03-01039a.

*alain.audouard@lncmi.cnrs.fr

[1] R. N. Lyubovskaia, O. A. Dyachenko, V. V. Gritsenko, S. G. Mkoyan, L. O. Atovmyan, R. B. Lyubovskii, V. N. Laukhin, A. V. Zvarykina, and A. G. Khomenko, Synth. Met. **42**, 1907 (1991).

[2] O. A. D'yachenko, V. V. Gritsenko, S. G. Mkoyan, G. V. Shilov, and L. O. Atovmyan, Russ. Chem. Bull. **40**, 1825 (1991).

[3] O. A. Dyachenko, V. V. Gritsenko, and R. N. Lyubovskaya, Russ. Chem. Bull. **45**, 370 (1996).

[4] R. Lyubovskaya, O. Dyachenko, and R. Lyubovskii, Synth. Met. **56**, 2899 (1993).

[5] L. F. Veiros and E. Canadell, J. Phys. I (France) **4**, 939 (1994).

[6] D. Vignolles, A. Audouard, R. B. Lyubovskii, M. Nardone, E. Canadell, E. I. Zhilyaeva, and R. N. Lyubovskaya, Eur. Phys. J. B **66**, 489 (2008).

[7] C. Proust, A. Audouard, L. Brossard, S. I. Pesotskii, R. B. Lyubovskii, and R. N. Lyubovskaia, Phys. Rev. B **65**, 155106 (2002).

[8] D. Vignolles, A. Audouard, L. Brossard, S. Pesotskii, R. Lyubovskii, M. Nardone, E. Haanappel, and R. Lyubovskaya, Eur. Phys. J. B **31**, 53 (2003).

[9] A. Audouard, D. Vignolles, E. Haanappel, I. Sheikin, R. B. Lyubovskii, and R. N. Lyubovskaya, Europhys. Lett. **71**, 783 (2005).

[10] J. Y. Fortin and A. Audouard, Phys. Rev. B **77**, 134440 (2008).

[11] R. Lyubovskii, S. Pesotskii, R. Lyubovskaya, E. Zhilyaeva, and O. Bogdanova, JETP Lett. **89**, 583 (2009).

[12] J. Singleton, C. de la Cruz, R. D. McDonald, S. Li, M. Altarawneh, P. Goddard, I. Franke, D. Rickel, C. H. Mielke, X. Yao, and P. Dai, Phys. Rev. Lett. **104**, 086403 (2010).

[13] H. Shishido, A. F. Bangura, A. I. Coldea, S. Tonegawa, K. Hashimoto, S. Kasahara, P. M. C. Rourke, H. Ikeda, T. Terashima, R. Settai, Y. Omacrnuki, D. Vignolles, C. Proust, B. Vignolle, A. McCollam, Y. Matsuda, T. Shibauchi, and A. Carrington, Phys. Rev. Lett. **104**, 057008 (2010).

[14] CRYSALISPRO, Version 1.171.33.66 (Oxford Diffraction Ltd., Abingdon, UK, 2010).

[15] A. Altomare, G. Cascarano, C. Giacovazzo, and A. Guagliardi, J. Appl. Crystallogr. **26**, 343 (1993).

[16] V. Petricek, M. Dusek, and L. Palatinus, *JANA2006. The Crystallographic Computing System* (Institute of Physics, Praha, Czech Republic, 2006).

[17] M.-H. Whangbo and R. Hoffmann, J. Am. Chem. Soc. **100**, 6093 (1978).

[18] J. Ammeter, H.-B. Bürgi, J. Thibeault, and R. Hoffmann, J. Am. Chem. Soc. **100**, 3686 (1978).

[19] D. Vignolles, A. Audouard, R. B. Lyubovskii, S. I. Pesotskii, J. Béard, E. Canadell, G. V. Shilov, O. A. Bogdanova, E. I. Zhilayeva, and R. N. Lyubovskaya, Solid State Sci. **9**, 1140 (2007).

[20] M. Nardone, A. Audouard, D. Vignolles, and L. Brossard, Cryogenics **41**, 175 (2001).

[21] L. V. Zorina, T. G. Prokhorova, S. S. Khasanov, S. V. Simonov, V. N. Zverev, A. V. Korobenko, A. V. Putrya, V. S. Mironov, E. Canadell, R. P. Shibaeva, and E. B. Yagubskii, Cryst. Eng. Comm. **11**, 2102 (2009).

[22] V. N. Zverev, M. V. Kartsovnik, W. Biberacher, S. S. Khasanov, R. P. Shibaeva, L. Ouahab, L. Toupet, N. D. Kushch, E. B. Yagubskii, and E. Canadell, Phys. Rev. B **82**, 155123 (2010).

[23] M. H. Whangbo, J. M. Williams, P. C. W. Leung, M. A. Beno, T. J. Emge, and H. H. Wang, Inorg. Chem. **24**, 3500 (1985).

[24] T. F. Stalcup, J. S. Brooks, and R. C. Haddon, Phys. Rev. B **60**, 9309 (1999).

[25] J. Merino and R. H. McKenzie, Phys. Rev. B **62**, 2416 (2000).

[26] P. Limelette, P. Wzietek, S. Florens, A. Georges, T. A. Costi, C. Pasquier, D. Jérome, C. Mézière, and P. Batail, Phys. Rev. Lett. **91**, 016401 (2003).

[27] C. Strack, C. Akinci, V. Pashchenko, B. Wolf, E. Uhrig, W. Assmus, M. Lang, J. Schreuer, L. Wiehl, J. A. Schlueter, J. Wosnitza, D. Schweitzer, J. Muller, and J. Wykhoff, Phys. Rev. B **72**, 054511 (2005).

[28] A. Audouard, C. Jaudet, D. Vignolles, R. Liang, D. A. Bonn, W. N. Hardy, L. Taillefer, and C. Proust, Phys. Rev. Lett. **103**, 157003 (2009).

[29] Recall that this latter frequency corresponds to an orbit that is forbidden within the semiclassical model of coupled-orbit networks, although it is observed in (Cl, Cl) and (Cl, Br).[7–9]

[30] In the case where Bragg reflections are involved in a MB orbit, the parameter A_a/R_T goes to a maximum at a field $B_{\max}$, which should be lower than the maximum field reached in the experiment in order to derive a reliable B_0 value. For the a oscillations that involve four Bragg reflections, $B_{\max} = B_0/\ln(1+B_0 e\hbar/2\pi^2 k_B m_e m_a^* T_D)$,[31] which leads to $B_{\max}$ as high as 56 T for the data at 1.0 GPa.

[31] D. Vignolles, A. Audouard, V. N. Laukhin, J. Béard, E. Canadell, N. G. Spitsina, and E. B. Yagubskii, Eur. Phys. J. B **55**, 383 (2007).